



Stokes' third problem for Herschel–Bulkley fluids



Christophe Ancey*, Belinda M. Bates

Environmental Hydraulics Laboratory, École Polytechnique Fédérale de Lausanne, EPFL ENAC IIC LHE, Btiment GC (Station 18), Lausanne CH-1015, Switzerland

ARTICLE INFO

Article history:

Received 2 August 2016

Revised 18 March 2017

Accepted 25 March 2017

Available online 27 March 2017

Keywords:

Herschel–Bulkley fluids

Stokes problem

Lubrication theory

Shear flow

Depth-averaged equations

ABSTRACT

Herschel–Bulkley materials can be set in motion when a sufficiently high shear stress or body force is applied to them. We investigate the behaviour of a layer of Herschel–Bulkley fluid when it is suddenly tilted and subject to gravitational forces. The material's dynamic response depends on the details of its constitutive equation. When its rheological behaviour is viscoelastoplastic with no thixotropic behaviour, the material is set in motion instantaneously along its entire base. When its rheological behaviour involves two yield stresses (static and dynamic yield stresses), the material must be destabilised before it starts to flow. This problem is thus similar to a Stefan problem, with an interface that separates the sheared and unsheared regions and moves from top to bottom. We estimate the time needed to set the layer in motion in both cases. We also compare the solution to the local balance equations with the solution to the depth-averaged mass and momentum equations and show that the latter does not provide consistent solutions for this flow geometry.

© 2017 Published by Elsevier B.V.

1. Introduction

Viscoplastic fluid theory has long been used to approximate the complex rheological behaviour of natural materials such as snow and mud, particularly their transition between solid- and fluid-like states [1]. The theory's strength lies in its capacity to describe flow initiation and cessation using a single constitutive equation. Natural materials can also entrain the bed on which they flow and, in this case, it is tempting to see basal entrainment as a form of yielding induced by the passage of the flow [2–4].

Various processes are at work when bed materials are set in motion. Among these, two are expected to play a major part: the increase in the normal and shear stresses applied to the bed surface, and the decrease in the shear strength relative to gravitational forces. The first process is certainly the easiest to investigate experimentally and theoretically. The Stokes problem provides a theoretical perspective: fluid is set in motion by applying a shear stress to its boundary or by moving that boundary at a constant velocity [5,6]. The second process can be studied by suddenly applying a body force to the fluid initially at rest. For convenience, this paper refers to this problem as Stokes' third problem. For Newtonian fluids, there exists a similarity solution to this problem, which shows that the fluid is instantaneously set in motion and virtually all of the fluid layer is entrained even though the effects far

from the boundary are exponentially small [6]. Herschel–Bulkley materials display a more complex dynamic response to a sudden change in the stress state than do Newtonian fluids. This is because of their ability to remain static when the stress state lies below a certain threshold, although they yield when the stress state moves above it. This paper investigates Stokes' third problem for Herschel–Bulkley fluids.

The key issue in Stokes' first and third problems is the existence of an interface separating the yielded and unyielded flows. If this interface exists, then one should be able to determine its propagation velocity and, thereby, the entrainment rate (at least in ideal cases, such as Stokes' problems). For Stokes' first problem and classic Herschel–Bulkley materials, there is no interface and the material is set in motion instantaneously over its whole depth [7,8]. For Stokes' third problem and Herschel–Bulkley materials exhibiting thixotropy, recent studies have posited the existence of interfaces moving at constant velocity [2,3], but the formal proof is lacking.

The problem of determining entrainment rates has also been addressed within the framework of depth-averaged equations (see [9] for a review). As the mass and momentum balance equations are averaged, the interface between sheared and unsheared flows is systematically treated as a shock wave (its propagation velocity must satisfy the Rankine–Hugoniot equation regardless of the constitutive equation, see Section 2.1). Although depth-averaging leads to governing equations that are simpler to solve, they are not closed. The governing equations must be supplemented by closure equations that specify how local variables (such as the bottom

* Corresponding author.

E-mail address: christophe.ancey@epfl.ch (C. Ancey).

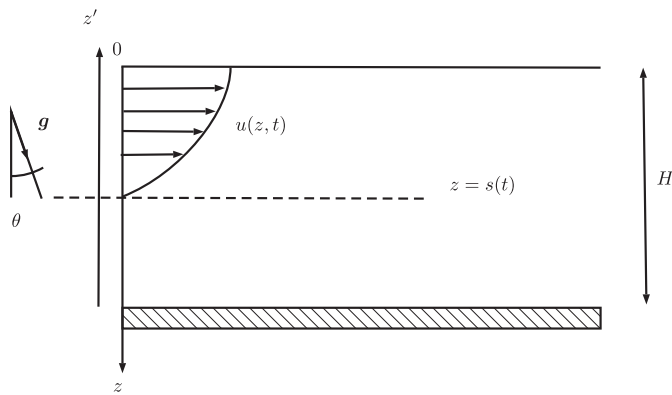


Fig. 1. Setting in motion a volume of fluid suddenly tilted at an angle θ .

shear stress and the entrainment rate) are related to bulk quantities (such as the depth-averaged velocity and flow depth). To date, most closure equations for non-Newtonian fluids have been based on empirical considerations and thus lack consensus [9].

This paper's objective is to explore the possibility of fluid-solid interfaces for Stokes's third problem and Herschel–Bulkley fluids. It is the continuation of previous studies devoted to Stokes' first [7,8] and second [10] problems. We begin by setting out what we refer to as Stokes' third problem (Section 2). We focus on Herschel–Bulkley fluids and outline the current state of the art in modelling Herschel–Bulkley fluids. The paper strays from the classic form of the Herschel–Bulkley constitutive equation in order to take advantage of recent developments in the rheometrical investigation of viscoplastic materials. Indeed, the classic form assumes that the material behaves like a rigid body when the stress state is below a given threshold, whereas in basal entrainment problems we expect the material's behaviour in its solid state to affect the entrainment dynamics. Our literature review led us to consider two types of Herschel–Bulkley fluids: simple Herschel–Bulkley fluids, whose rheological behaviour is well described by a one-to-one constitutive equation, and non-simple Herschel–Bulkley fluids, whose rheological behaviour exhibits shear-history dependence. We demonstrate that the details of the constitutive equation have a great deal of influence on the solution to Stokes' third problem. In Section 3, which is devoted to simple Herschel–Bulkley fluids, we show that the material is set in motion instantaneously. By contrast, non-simple Herschel–Bulkley materials do not start moving spontaneously; they must first be destabilised. A front subsequently propagates through the static layer and sets it in motion (Section 4). For non-simple Herschel–Bulkley materials, we also show that in the absence of slip, the depth-averaged equations do not require a closure equation for the entrainment rate, but the solution to these equations is physically inconsistent.

2. Stokes' third problem

The literature refers to two Stokes problems. Stokes' first problem refers to the impulsive motion of a semi-infinite volume of Newtonian fluid sheared by an infinite solid boundary. Stokes' second problem concerns the cyclical motion of this volume sheared by an oscillatory boundary [6]. These two problems have also been investigated for viscoplastic materials [7,8,10].

A related problem concerns the setting in motion of a layer of fluid of depth H , initially at rest and suddenly tilted at an angle θ to the horizontal (see Fig. 1). Contrary to the two Stokes problems above, we consider a volume that is not bounded by an infinite plate, but by a free surface. As this problem bears some resemblance to the original Stokes problem, this paper refers to it as Stokes' third problem (mainly for convenience). Previously, it

was partially studied for Herschel–Bulkley flows [2,3] and Drucker–Prager fluid [4].

2.1. Governing equations

We consider an incompressible Herschel–Bulkley fluid with density ρ ; its constitutive equation is discussed in Section 2.2. The fluid is initially at rest. There is a free surface located at $z = 0$, with the z -axis normal to the free surface and pointing downward. We also introduce the z' -axis, normal to the free surface, but pointing upward. The x -axis is parallel to the free surface. At time $t = 0$, the volume is instantaneously tilted at an angle θ to the horizontal. We assume that a simple shear flow takes place under the effects of gravitational forces and that the flow is invariant under any translation in the x -direction. The initial velocity is

$$u(z, 0) = 0. \quad (1)$$

At the free surface $z = 0$, in the absence of traction, the shear stress τ is zero

$$\tau = 0 \text{ at } z = 0. \quad (2)$$

A key issue in Stokes' third problem is the existence of a propagation front $z = s(t)$ (i.e. a moving interface between the sheared and stationary layers) and the boundary conditions at this front. For Stokes' first problem, shear-thinning viscoplastic fluids behave like Newtonian fluids: the momentum balance equation reduces to a linear parabolic equation, and the front propagates downward instantaneously [7,8]. The question arises as to whether this is also the case for Stokes' third problem.

Let us admit that the interface moves at a finite velocity v_f . The dynamic boundary condition at this interface is given by a Rankine–Hugoniot equation

$$\llbracket -\rho \mathbf{u}(\mathbf{u} \cdot \mathbf{n} - v_f) + \boldsymbol{\sigma} \cdot \mathbf{n} \rrbracket = 0, \quad (3)$$

where $\llbracket f \rrbracket$ denotes f 's jump across the interface [11,12]. In the absence of slip

$$\mathbf{u} = 0 \text{ at } z = s(t), \quad (4)$$

this equation implies the continuity of the stresses across the interface

$$\llbracket \tau \rrbracket = 0 \text{ and } \llbracket \sigma_{zz} \rrbracket = 0, \quad (5)$$

where σ_{zz} is the normal stress in the z -direction. If the material slips along the bed-flow interface at a velocity u_s , then the Rankine–Hugoniot equation implies that the shear stress exhibits a jump across the interface, while the normal stress is continuous

$$\llbracket \tau \rrbracket = -\rho u_s v_f \text{ and } \llbracket \sigma_{zz} \rrbracket = 0.$$

The first relationship has often been used in the form $v_f = -\llbracket \tau \rrbracket / (\rho u_s)$, which fixes the entrainment rate when the other variables are prescribed [3,13,14]. Internal slip in viscoplastic materials is only partially understood. It may be a consequence of shear localisation or shear banding in thixotropic viscoplastic fluids [15,16]. In the rest of the paper, we assume that the no-slip condition applies at the interface, and so the boundary condition is given by equation (5).

For this problem, the governing equation is derived from the momentum balance equation in the x -direction

$$\rho \frac{\partial u}{\partial t} = \rho g \sin \theta - \frac{\partial \tau}{\partial z}. \quad (6)$$

To solve the initial boundary value problem (2)–(6), we need to specify the constitutive equation.

2.2. Constitutive equation

For simple shear-flows, the Herschel–Bulkley constitutive equation reads

$$\begin{cases} \dot{\gamma} = 0 & \text{if } \tau < \tau_c, \\ \tau = \tau_c + \kappa |\dot{\gamma}|^n & \text{if } \tau \geq \tau_c, \end{cases} \quad (7)$$

where τ_c denotes the yield stress, $\dot{\gamma} = du/dz$ the shear rate, n the shear-thinning index (as in most cases $n \leq 1$) and κ the consistency. This equation essentially relies on a phenomenological basis. A tensorial equation can be derived by using a von Mises yield criterion to define the yield surface (i.e. the surface separating sheared from unshaded regions) [1]. The interpretation of Eq. (7) is classic: for the material to flow, the shear stress τ must exceed a threshold τ_c , called the yield stress. When $\tau < \tau_c$, the material remains unshaded.

The existence of a true yield stress was long debated. It is now well accepted that for a class of fluids referred to as *simple yield-stress fluids*, Eq. (7) closely describes the rheological behaviour in steady-state simple-shear flows [17,18], and in a tensorial form, the Herschel–Bulkley equation offers a correct approximation of three-dimensional flows, notably with regards to the von Mises criterion for yielding [19]. This means that for these fluids in steady state viscometric flows, the shear rate tends continuously to zero when the shear stress approaches the yield stress. For non-simple yield stress fluids, e.g. those exhibiting thixotropy, the shear rate cannot be given a value when $\tau \rightarrow \tau_c$: indeed, there may be no homogeneous steady-state flow when the shear rate drops below a finite critical value $\dot{\gamma}_c$ [17–22]. This also entails that the material exhibits a static yield stress $\tau_0 > \tau_c$ that differs from the dynamic yield stress τ_c in Eq. (7). The steady state constitutive equation reads

$$\tau = \tau_c + \kappa |\dot{\gamma}|^n \text{ if } |\dot{\gamma}| \geq \dot{\gamma}_c, \quad (8)$$

with $\tau_0 = \tau_c + \kappa \dot{\gamma}_c^n$. For $0 < |\dot{\gamma}| \leq \dot{\gamma}_c$, the rheological behaviour exhibits complex properties (time dependency, a thixotropy loop, shear banding, aging and shear rejuvenation, or minimum in the flow curve) depending on the material [16–18]. Various approaches have been proposed to incorporate the effect of shear history in the constitutive equation, but a general framework of the underlying mechanisms is still lacking [16,20,23,24]. For the sake of simplicity, we assume that as the shear rate increases from zero, the shear stress must exceed τ_0 for a steady state flow to occur. When the shear rate decreases from a sufficiently high value in a steady-state regime, the shear stress follows the flow curve (7) continuously even for $|\dot{\gamma}| < \dot{\gamma}_c$ [21,25–27]. Thus, flow cessation and fluidisation cannot be described by a one-to-one constitutive equation.

Prior to yielding, a Herschel–Bulkley material is often considered to behave like an elastic solid. A simple idea is then to supplement the constitutive equation (7) with an equation reflecting the elastic behaviour for $\tau < \tau_c$, but this leads to inconsistencies such as the non-uniqueness of the yield function due to finite deformations (and thus normal stresses) in the solid material [28]. One alternative is to use a viscoelastoplastic constitutive equation [29], which extends Oldroyd's viscoelastic model to plastic materials [30]. Although the model is consistent from a continuum mechanics' point of view and experimentally [31], it involves nontrivial differential operators (Gordon–Schowalter derivatives), which make analytical calculations intricate. Here, we follow Lacaze et al. [32], who suggested neglecting the nonlinear differential terms in order to end up with an approximate constitutive equation for simple shear flows

$$\frac{1}{G} \frac{\partial \tau}{\partial t} = \dot{\gamma} - \max \left(0, \frac{|\tau| - \tau_c}{\kappa |\tau|^n} \right)^{1/n} \tau, \quad (9)$$

where G is the elastic modulus. Under steady state conditions, this equation leads to the Herschel–Bulkley model (7).

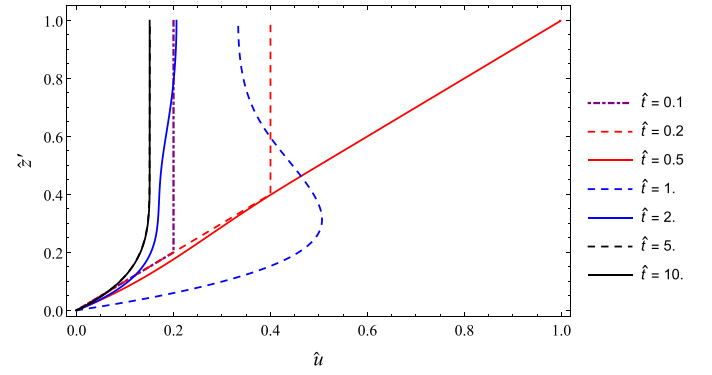


Fig. 2. Evolution of the velocity profile for $De = 0.1$, $Re = 10$, $Bi = 0.5$ and $n = 1/3$. We report the computed velocity profiles at times $\hat{t} = 0.1, 0.2, 0.5, 1, 2, 5$ and 10 . Numerical simulation with $N = 1000$ nodes.

3. Solution to Stokes' third problem for simple Herschel–Bulkley fluids

3.1. Dimensionless governing equations

We introduce the following scaled variables

$$u \rightarrow U_* \hat{u}, \quad z \rightarrow H_* \hat{z}, \quad t \rightarrow T_* \hat{t}, \quad \text{and} \quad \tau \rightarrow \frac{\mu U_*}{H_*} \hat{\tau} \quad (10)$$

with $U_* = \rho g H^2 \sin \theta / \mu$ the velocity scale, $H_* = H$ the length scale, $T_* = H_* / U_*$ the time scale, $\mu = \kappa (U_* / H_*)^{n-1}$ the bulk viscosity. We also introduce the Reynolds, Bingham and Deborah dimensionless numbers

$$Re = \frac{\rho U_* H_*}{\mu}, \quad Bi = \frac{\tau_c}{\mu \frac{U_*}{H_*}}, \quad \text{and} \quad De = \frac{\mu U_*}{G H_*}. \quad (11)$$

The governing equations reduce to a nonhomogeneous linear hyperbolic problem

$$Re \frac{\partial \hat{u}}{\partial \hat{t}} = 1 + \frac{\partial \hat{\tau}}{\partial \hat{z}'}, \quad (12)$$

$$De \frac{\partial \hat{\tau}}{\partial \hat{t}} = \frac{\partial \hat{u}}{\partial \hat{z}'} - F(\hat{\tau}), \quad (13)$$

with $F(\hat{\tau}) = \max(0, |\hat{\tau}| - Bi)^{1/n} \hat{\tau} / |\hat{\tau}|$. The boundary and initial conditions are $\hat{u} = 0$ at $\hat{z}' = 0$, $\hat{\tau} = 0$ at $\hat{z}' = 1$, and $\hat{\tau} = \hat{u} = 0$ at $\hat{t} = 0$. The analysis of the associated characteristic problem shows that the material starts moving at its base instantaneously when the initial thickness H is sufficiently large, i.e. for $Bi < 1$ (see Appendix A). The disturbance propagates toward the free surface at velocity $\hat{c} = 1/\sqrt{ReDe}$. The time of setting in motion is defined here as the time

$$\hat{t}_c = 1/\hat{c} = \sqrt{ReDe} \quad (14)$$

needed for this disturbance to reach the free surface. If we use the traditional form (7) for the Herschel–Bulkley constitutive equation (i.e. with a rigid behaviour for $\tau < \tau_c$), then this time drops to zero as $G \rightarrow \infty$ and $De \rightarrow 0$. In the absence of elastic behaviour, no relaxation phase occurs and the setting in motion is instantaneous (the velocity profile also matches the steady state profile instantaneously).

3.2. Numerical solutions

Numerical solutions to the problem (12)–(13) can be obtained using the method of characteristics (see Appendix A). Fig. 2 shows an example of the evolution of the velocity profile for a particular set of values of De , Re , Bi and n . In short time periods ($\hat{t} < \hat{t}_c$), the

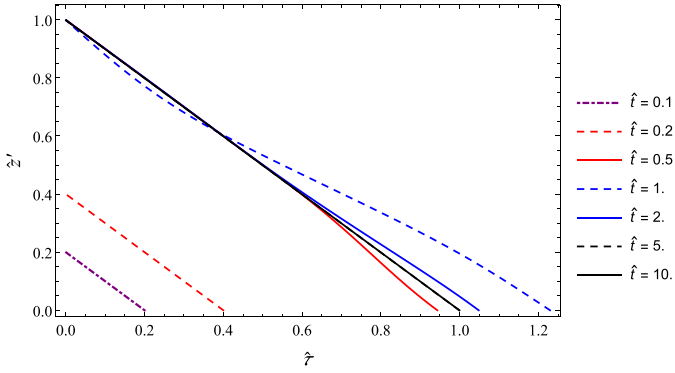


Fig. 3. Evolution of the shear-stress profile for $De = 0.1$, $Re = 10$, $Bi = 0.5$ and $n = 1/3$. We report the computed velocity profiles at times $\hat{t} = 0.1, 0.2, 0.5, 1, 2, 5$ and 10 .

material starts deforming along its base and accelerating as a result of the body force. The velocity varies linearly close to the bottom, whereas the upper layers of the material remain unsheared. At $\hat{t} = \hat{t}_c$, the initial disturbance reaches the free surface and the entire depth is now sheared. For \hat{t} slightly longer than t_c , there is a phase of elastic adjustment, reflected by a strong deceleration (by a factor of 5 in Fig. 2) and a bumpy velocity profile. At longer time periods ($\hat{t} > 5\hat{t}_c$), the velocity approaches its steady-state profile, characterised by a shear region for $\hat{z}' \leq Bi$ and a plug flow for $\hat{z}' > Bi$.

Fig. 3 shows the stress evolution. At short time periods ($\hat{t} < \hat{t}_c$), the shear stress varies linearly near the bottom and is zero in the upper layers. The elastic adjustment phase entails the propagation of shear waves that dampen quickly. At long time periods ($\hat{t} > \hat{t}_c$), the shear stress is close to its steady state profile $\hat{\tau} = 1 - \hat{z}'$.

4. Solution to Stokes' third problem for non-simple Herschel–Bulkley fluids

When the fluid exhibits a static yield stress τ_0 that is larger than its dynamic yield stress τ_c , it is sufficiently rigid to stand sudden tilting without deforming instantaneously as long as $\tau_0 > \rho g H \sin \theta$. However, in such a case, if the material is destabilised locally (see below), a front may propagate downwards from the point of destabilisation. This is the result of the fluid's destructure during yielding. For the sake of simplicity, we focus on a Bingham fluid ($n = 1$), the results of which can be easily extended to Herschel–Bulkley fluids.

We consider a thixotropic Bingham fluid, whose constitutive equation depends on its shear history, as follows (see Section 2.2 and Fig. 4) [15]

$$\begin{cases} \dot{\gamma} = 0 & \text{if } \tau < \tau_c, \\ \tau = \tau_c + \kappa |\dot{\gamma}| & \text{if } \tau \geq \tau_0 \text{ for increasing } \dot{\gamma}, \\ \tau = \tau_c + \kappa |\dot{\gamma}| & \text{if } \tau \geq \tau_c \text{ for decreasing } \dot{\gamma}. \end{cases} \quad (15)$$

In Stokes' third problem, when the layer is suddenly tilted, the shear stress adopts a linear profile in the absence of motion (i.e. when the material behaves like a rigid body): $\tau(z) = \rho g z \sin \theta$. If the layer thickness exceeds the critical depth $h_0 = \tau_0 / (\rho g \sin \theta)$, the whole layer is set in motion instantaneously because its base yields instantaneously (see Section 3). We therefore consider layers whose thickness H satisfies $h_0 > H > h_c$ with $h_c = \tau_c / (\rho g \sin \theta)$. If this layer is not disturbed, it will stay at rest indefinitely. Contrary to the previous section, we need to alter the initial condition in order to create motion. There are many ways of doing so and, therefore, many initial boundary value problems can be addressed depending on the initial velocity disturbance and stresses applied to the boundaries. Here, we consider the simplest case, in which

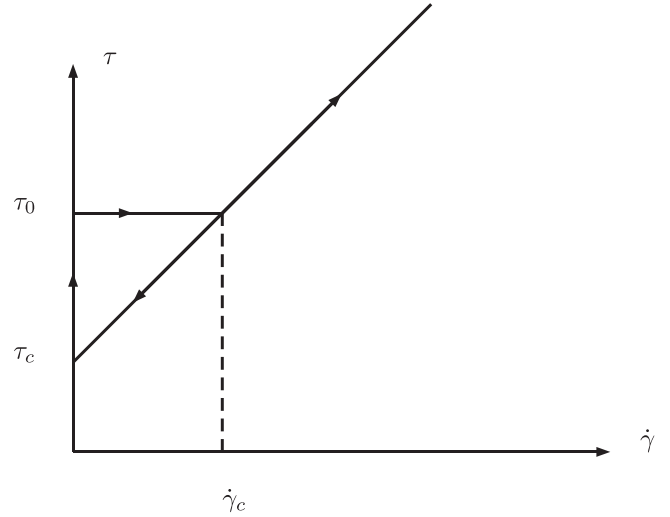


Fig. 4. Flow curve. We assume that when the material is at rest, it behaves like a rigid body. When the shear stress exceeds a threshold called the static yield stress τ_0 , it starts moving, but until the shear rate exceeds a critical shear-rate $\dot{\gamma}_c$, there is no steady state. When the shear rate is increased above this critical value, the material behaves like a Bingham fluid. If the shear rate is decreased from a value $\dot{\gamma} > \dot{\gamma}_c$, then the shear stress follows another path marked by the down arrow. In that case, it can approach the zero limit continuously, when the shear stress comes closer to the static yield stress τ_c . Inspired from Ovarlez et al. [15].

we apply a constant shear stress τ_c at the free surface (so that the whole layer is prone to yielding) and we impose an initial velocity disturbance, which is necessary to destabilise the layer. If the shear stress applied at the bottom surface is lower than τ_c , then a plug (unsheared) layer quickly forms between the free surface and shear flow, and we thus have to track two interfaces: one corresponding to $\tau = \tau_0$ (bed erosion) and the other to $\tau = \tau_c$ (plug layer), which makes the problem more complicated. So, in the following subsection, we will not address every possible boundary condition, but merely focus on a simple case. Furthermore, we will show that the initial velocity disturbance cannot be arbitrary, but must satisfy certain constraints for the interface to propagate through the static layer (see Section 4.2).

4.1. Dimensionless governing equations

We make the problem dimensionless using the same scales as in Section 3. The dimensionless initial boundary value problem is

$$Re \frac{\partial \hat{u}}{\partial \hat{t}} = 1 + \frac{\partial^2 \hat{u}}{\partial \hat{z}^2}, \quad (16)$$

subject to the boundary conditions at the free surface $\hat{z} = 0$

$$\frac{\partial \hat{u}}{\partial \hat{z}}(0, \hat{t}) = 0. \quad (17)$$

There is a moving boundary at $\hat{z} = \hat{s}(\hat{t})$ for which the no-slip condition holds

$$\hat{u}(\hat{s}, \hat{t}) = 0 \quad (18)$$

while the stress continuity (5) across this interface gives

$$\frac{\partial \hat{u}}{\partial \hat{z}}(\hat{s}, \hat{t}) = -\hat{\gamma}_c \text{ with } \hat{\gamma}_c = \hat{\tau}_0 - Bi > 0. \quad (19)$$

The initial condition is

$$\hat{u}(\hat{z}, 0) = \hat{u}_0(\hat{z}) \text{ for } 0 \leq \hat{z} \leq \hat{s}_0, \quad (20)$$

with $\hat{u}_0 > 0$. For the initial and boundary conditions to be consistent, we also assume that $\hat{u}'_0(0) = 0$ and $\hat{u}'_0(\hat{s}_0) = -\hat{\gamma}_c$.

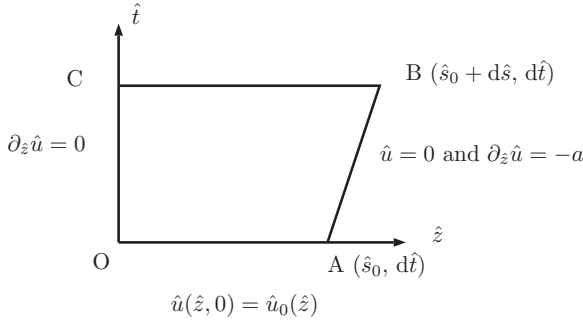


Fig. 5. Incipient motion around point O (0, 0). At time $t = 0$, we impose a velocity profile (20) to the layer $0 \leq \hat{z} \leq \hat{s}_0$, and so that the front is initially at point A. At time $d\hat{t}$, the front has reached point B located at $\hat{s} + d\hat{s}$. Along segments OC and AB, boundary conditions (17), and (18) together with (19) apply, respectively.

This initial boundary value problem is close to the Stefan problem, which describes the evolution in temperature within a medium experiencing a phase transition. As in the Stefan problem, the evolution equation (16) is a linear parabolic equation, but the whole system of equations is nonlinear [33]; this results from the existence of a moving boundary $\hat{s}(\hat{t})$, which has to be determined while solving the system (16)–(19). The present problem shows two crucial differences from the Stefan problem: firstly, there is a source term in the diffusion equation (16), and secondly, the position $\hat{s}(\hat{t})$ of the moving boundary does not appear explicitly in Eqs. (16)–(19). These two differences have crucial effects on the solution, notably the existence of a solution at all times. We address this point in the next subsection.

4.2. Existence of a solution

Contrary to the Stefan problem, the moving boundary $\hat{s}(\hat{t})$ will not start moving spontaneously. Part of the fluid must be destabilised prior to incipient motion, and that is the meaning of the initial condition (20). This is also consistent with the thixotropic behaviour described by constitutive equation (15).

To show this, let us consider what happens in the earliest moments of motion by using the Green theorem. Initially the interface position is at $\hat{s}(0) = \hat{s}_0$ (point A in Fig. 5), and after a short time $\Delta\hat{t}$, it has moved to $\hat{s}_0 + d\hat{s}$ (point B in Fig. 5). The displacement increment can be determined by differentiating the boundary condition (18)

$$\frac{d}{d\hat{t}} \hat{u}(\hat{s}, \hat{t}) = \left. \frac{\partial \hat{u}}{\partial \hat{z}} \right|_{\hat{s}} \frac{d\hat{s}}{d\hat{t}} + \left. \frac{\partial \hat{u}}{\partial \hat{t}} \right|_{\hat{s}} = 0. \tag{21}$$

Using evolution equation (16) and boundary condition (19), we deduce

$$\hat{\gamma}_c \left. \frac{d\hat{s}}{d\hat{t}} \right|_0 = \frac{1 + u_0''(\hat{s}_0)}{\text{Re}}. \tag{22}$$

We then deduce that the front has moved a distance $d\hat{s} = (1 + u_0''(\hat{s}_0))d\hat{t}/(\hat{\gamma}_c \text{Re})$.

Applying the Green theorem to the oriented surface OABC gives

$$\oint_{\text{OABC}} \left(\text{Re} \frac{\partial \hat{u}}{\partial \hat{t}} - \frac{\partial^2 \hat{u}}{\partial \hat{z}^2} \right) d\hat{z}d\hat{t} = \int_{\text{OABC}} \text{Re} \hat{u} d\hat{z} + \frac{\partial \hat{u}}{\partial \hat{z}} d\hat{t}.$$

The only condition on the path CB is that the velocity must be positive: $\int_{\text{CB}} \hat{u} d\hat{z} > 0$. Making use of boundary conditions (17)–(19) and initial condition (20), we find the necessary condition for motion

$$\int_0^{\hat{s}_0} \hat{u}_0 d\hat{z} > \frac{\hat{\gamma}_c + \hat{s}_0}{\text{Re}} d\hat{t} + \frac{1 + u_0''(\hat{s}_0)}{2\hat{\gamma}_c \text{Re}} d\hat{t}^2. \tag{23}$$

However, no solution satisfies this condition in the limit $s_0 \rightarrow 0$. A sufficiently high shear must be applied to the upper layer over a thickness \hat{s}_0 for the flow to start.

4.3. Similarity solution

There is no exact similarity solution to the problem of equations (16)–(19), but we can work out an approximate solution which describes the flow behaviour in the vicinity of the interface $\hat{s}(\hat{t})$. To that end, we seek a solution in the form $\hat{u}(\hat{z}, \hat{t}) = \hat{t}F(\xi, \hat{t})$, with $\xi = \hat{z}/\hat{t}$ as the similarity variable. Substituting \hat{u} in this form into governing equation (16) gives

$$\text{Re}F(\xi, \hat{t}) + \text{Re}\hat{t} \frac{\partial F}{\partial \hat{t}} = \text{Re}\xi \frac{\partial F}{\partial \xi} + 1 + \frac{1}{\hat{t}} \frac{\partial^2 F}{\partial \xi^2}. \tag{24}$$

We then use the expansion $F(\xi, \hat{t}) = F_0(\xi) + \hat{t}^{\nu_1}F_1(\xi) + \dots + \hat{t}^{\nu_i}F_i(\xi) + \dots$, with F_i functions of ξ alone and $\nu_i > 0$. To leading order and in the limit $\hat{t} \gg 1$, Eq. (24) can be reduced to a first order differential equation

$$\text{Re}F_0 = 1 + \text{Re}\xi F_0', \tag{25}$$

subject to $F(\xi_f) = 0$ and $F'(\xi_f) = -\hat{\gamma}_c$, where $\xi_f = \hat{s}/\hat{t}$ is the position of the interface. The solution is

$$F_0 = \frac{1}{\text{Re}} - \hat{\gamma}_c \xi. \tag{26}$$

The solution satisfies boundary conditions (18) and (19) at the interface, but not boundary condition (17) at the free surface. A boundary layer correction should be used to account for the influence of this boundary condition. As shown by the numerical solution in Section 4.4, the approximate similarity solution (26) offers a fairly good description of the solution, thus we will not go further in this direction.

From this calculation, we deduce that the interface behaves like a travelling wave, whose velocity is constant and fixed by the critical-shear rate: $\hat{v}_f = (\text{Re}\hat{\gamma}_c)^{-1}$. The interface position is then

$$\hat{s} = s_0 + \frac{\hat{t}}{\text{Re} \hat{\gamma}_c}. \tag{27}$$

The velocity profile is linear in the vicinity of the interface

$$\hat{u} = \frac{\hat{t}}{\text{Re}} - \hat{z}\hat{\gamma}_c. \tag{28}$$

It can easily be shown that the travelling wave’s structure does not depend on the shear-thinning index n . Indeed, the details of the constitutive equation affect the structure of the diffusive term in the momentum balance equation, however, in the vicinity of the interface, this contribution is negligible compared to the source term. Whatever the value of n , the time required for the interface to travel the distance $\hat{H} = 1$ is thus

$$\hat{t}_c \sim \text{Re} \hat{\gamma}_c. \tag{29}$$

4.4. Numerical solution

We used a finite-difference scheme to solve system (16)–(19) (see Appendix B for the details). In Figs. 6–8, we show an example of a simulation for $\hat{\tau}_c = \text{Bi} = 0.5$, $\hat{\tau}_0 = 1$, and thus $\hat{\gamma}_c = \hat{\tau}_0 - \text{Bi} = 0.5$. For the initial disturbance, we assumed that the velocity profile was

$$\hat{u} = \frac{\hat{\gamma}_c}{2} \hat{s}_0 \left(1 - \left(\frac{\hat{z}}{\hat{s}_0} \right)^2 \right),$$

with $\hat{s}_0 = 0.6$. The mesh size was $h = 10^{-3}$. This velocity profile satisfied boundary conditions (17)–(19). The initial thickness had to be selected such that the condition (23) was satisfied. Furthermore,

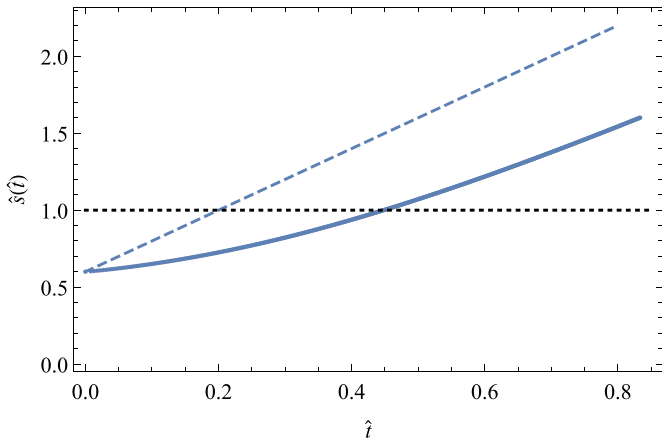


Fig. 6. Interface position $\hat{s}(\hat{t})$ over time. Initially, the interface is at $\hat{s}(0) = 0.6$. The solid line shows the numerical solution to system (16)–(19), whereas the dashed line represents approximate solution (27). The dotted line shows the position of the bottom $\hat{z} = 1$. The numerical solution was computed for $\hat{\gamma}_c = \hat{\tau}_0 - \text{Bi} = 0.5$ and $\text{Re} = 1$.

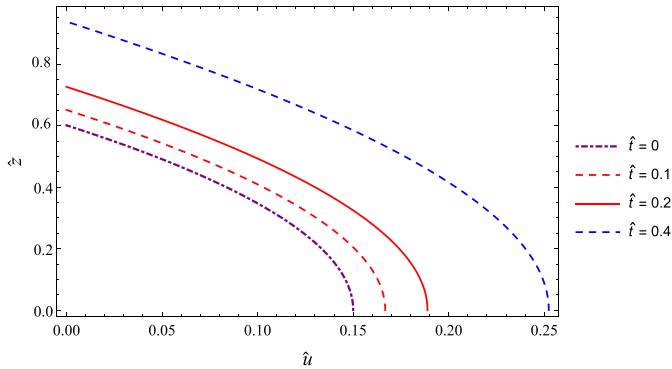


Fig. 7. Velocity profiles for $\hat{t} = 0, 0.1, 0.2$ and 0.4 . Numerical solution to Eqs. (16)–(19) for $\hat{\gamma}_c = \hat{\tau}_0 - \text{Bi} = 0.5$ and $\text{Re} = 1$.

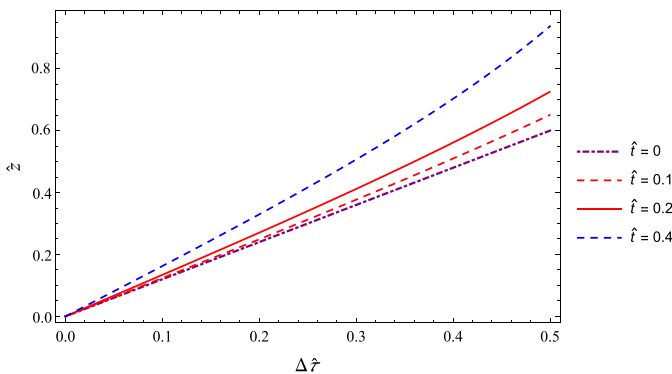


Fig. 8. Excess shear-stress profiles for $\hat{t} = 0, 0.1, 0.2$ and 0.4 . Numerical solution to Eqs. (16)–(19) for $\hat{\gamma}_c = \hat{\tau}_0 - \text{Bi} = 0.5$ and $\text{Re} = 1$. The excess shear stress is defined as $\Delta \hat{\tau} = \hat{\tau} - \hat{\tau}_c$.

the initial interface velocity $d\hat{s}_0/dt$ given by (22) implies that there is a lower bound \hat{s}_0 the initial interface velocity cannot be positive. Here, we found $\hat{s}_0 > \hat{\gamma}_c$. We therefore selected $\hat{s}_0 = 0.6$. As the initial layer had a thickness $\hat{z} = 1$, this means that 60% of the layer had to be destabilised for the interface to propagate downward.

Fig. 6 shows the interface position $\hat{s}(\hat{t})$ as a function of time. Analytical The curve given by analytical solution (27) is parallel to the numerical solution at later time periods (see Fig. B.11 for behaviour at later time periods), confirming that the disturbance grows and propagates as a travelling wave over sufficiently long

time periods. However, the convergence to the similarity solution may be slow (depending on the initial velocity), and the interface \hat{s} reaches the bottom $\hat{z} = 1$ before it converges to the similarity solution. Here, the bottom $\hat{z} = 1$ (indicated by the dotted line in Fig. 6) is reached at $\hat{t} = 0.44$, whereas the similarity solution gives the time $\hat{t} = 0.2$.

Fig. 7 shows the velocity profiles at different times. These profiles show that approximate similarity solution (28) provides a fairly good description of the velocity profile for 50% of the depth, but as the initial condition was a parabolic profile, this is not surprising. Fig. 8 shows the shear-stress profiles, which were obtained by the numerical integration of the numerical solution. The shear stress spans the range $[\hat{\tau}_c, \hat{\tau}_0]$ (as expected, considering the boundary conditions imposed) and exhibits a nonlinear profile (except for the initial time of disturbance, at which it is linear).

4.5. Comparison with earlier contributions

A few authors have addressed Stokes’ third problem in recent years. Eglit and Yakubenko [2] solved the problem for a non-simple Bingham fluid numerically. They regularised the constitutive equation by using a biviscous fluid. They observed that the interface moved as a travelling wave with velocity $v_f = \mu g \sin \theta / (\tau_0 - \tau_c)$, as we did, but their numerical simulations were not in full agreement with our results: they found that the thickness of the plug region grew indefinitely and that the interface velocity depended on consistency when the fluid was shear-thinning. The thickness of the plug region is usually considered to be bounded by $h_c = \tau_c / (\rho g \sin \theta)$ and thus not to grow indefinitely. We found that locally, the interface behaved like a travelling wave whose velocity depended solely on the stress difference $\Delta \tau = \tau_0 - \tau_c$, regardless of n . As Eglit and Yakubenko [2] did not give much detail to their numerical solution, it is difficult to appreciate the reasons for this disagreement.

Issler [3] investigated Stokes’ third problem for non-simple Herschel–Bulkley fluids but, to remove time dependence, he assumed that the mobilised material was of constant thickness. By assuming the existence of a travelling wave solution, he found an expression of the interface velocity v_f , but due to his working assumption, there is no agreement between his solution and our calculations.

Bouchut et al. [4] also studied Stokes’ third problem, but for plastic materials with a Drucker–Prager yield criterion (i.e. with a yield surface that depends on the first invariant of the stress tensor). They worked out an exact solution for purely plastic materials (i.e. with zero viscosity $\kappa = 0$) that showed that motion dies out quickly after an initial disturbance (this is in agreement with our condition for incipient motion in Section 4.2). They did not provide a closed-form analytical solution for the general case $\kappa > 0$.

4.6. Comparison with the solutions for depth-averaged equations

Here we consider the depth-averaged mass and momentum equations (C.4) and (C.7) derived in Appendix C. For the present flow geometry (no basal slip, invariance to any invariance in the x direction), a uniform layer grows in size in the z -direction, and these equations reduce to

$$\frac{dh}{dt} = v_f, \tag{30}$$

$$\frac{dh\bar{u}}{dt} = gh \sin \theta - \frac{\tau_b}{\rho}, \tag{31}$$

with τ_b the basal shear-stress approximated by Eq. (C.8), h the layer thickness, and \bar{u} the depth-averaged velocity. Boundary condition (5), at the base of the flowing layer, implies that

$$\tau_b = \tau_0 = \tau_c + 2\kappa \frac{\bar{u}}{f(h)} \quad (32)$$

with $f(h) = (h - h_c)(2 + h_c/h)/h$ given by Eq. (C.8). This boundary condition thus provides us with a relationship between h and \bar{u} :

$$\bar{u} = \frac{\Delta\tau}{2\kappa} f(h) \quad (33)$$

with $\Delta\tau = \tau_0 - \tau_c$.

In a dimensionless form, governing equations (30) and (31) can be cast in the form

$$\frac{d\hat{h}}{d\hat{t}} = \hat{v}_f, \quad (34)$$

$$\text{Re} \frac{d\hat{h}\hat{u}}{d\hat{t}} = \hat{h} - \hat{\tau}_0. \quad (35)$$

Introducing $F(\hat{h}) = \hat{u}\hat{h} = \Delta\hat{\tau}\hat{h}f(\hat{h})/2$, we can rewrite Eq. (35)

$$\text{Re} F'(\hat{h}) \frac{d\hat{h}}{d\hat{t}} = \hat{h} - \hat{\tau}_0, \quad (36)$$

and thereby, we end up with a differential equation for \hat{h}

$$\frac{d\hat{h}}{d\hat{t}} = \frac{1}{\text{Re}} \frac{\hat{h} - \hat{\tau}_0}{F'(\hat{h})}. \quad (37)$$

As $\text{Bi} < \hat{h} < \hat{\tau}_0$, we deduce that $\hat{h}' < 0$, which does not reflect the material's expected behaviour. The depth-averaged equations do not provide a consistent solution to our entrainment problem. In this section, we used the simplest closure equation for the bottom shear stress. As highlighted in Appendix C, there are more elaborate expressions for the bottom shear stress, but their use would not change the final outcome. Similarly, using empirical equations for the entrainment rates, as has been done in a number of geophysical models (see Iverson and Ouyang [9] for a discussion), would lead to inconsistencies in the governing equations (in the particular case addressed here, the system of equations would be overdetermined).

When diagnosing the failure of the depth-averaged equations, one obvious explanation is that boundary condition (32) makes the bottom shear-stress constant, and therefore the source term in the momentum balance equation (31) is negative. Furthermore, as boundary condition (32) also implies that the velocity is fixed by the flow depth, the depth-averaged equations lead to shrinking flow layers ($h'(t) < 0$), whereas thickening flowing layers are expected here.

5. Concluding remarks

In this paper, we investigated Stokes' third problem with the aim of calculating the speed of propagation of the interface separating static and flowing materials. For simple Herschel-Bulkley fluids, the base of the layer is unable to resist a shear stress and the material starts moving instantaneously. The characteristic time of motion (t_c) is then defined as the time needed for the initial disturbance to propagate from the bed to the free surface. We found that $\hat{t}_c = \sqrt{\text{ReDe}}$ or, dimensionally, $t_c = H\sqrt{\rho/G}$. In the traditional formulation for Herschel-Bulkley fluids, there is no associated viscoelastic behaviour. In other words, the elastic modulus G is infinite, thus $t_c = 0$ (instantaneous adjustment), and the fluid velocity profile reaches its steady state instantaneously. There is no significant difference between Stokes' first and third problems with regards to the existence of moving interfaces between sheared and unsheared regions.

For non-simple Herschel-Bulkley fluids, the material needs to be destabilised. Eq. (23) provides a necessary condition for the initial disturbance to create motion. Different solutions can be ob-

tained depending on the stress applied when creating this initial disturbance: there is thus no unique solution. In the particular initial boundary value problem studied here, we showed that the disturbance propagates down to the bottom and asymptotically reaches a constant velocity $\hat{v}_f = (\text{Re}\hat{\gamma}_c)^{-1}$. The time needed for the disturbance to cross the static layer is of the order $\hat{t}_c = (\text{Re}\hat{\gamma}_c)$ or, dimensionally, $t_c = O(H(\tau_0 - \tau_c)/(\mu g \sin \theta))$.

One important result of this study was to shed light on the role played by dynamic yield stress in a time-dependent problem like basal entrainment. When the dynamic and static yield stresses coincide and the fluid behaves like a viscoelastoplastic material, the governing equations are linear and hyperbolic: there is no moving boundary separating sheared and unsheared regions. The situation does not differ from that found for Stokes' first problem [7,8] except that in the present case, even shear-thickening fluids ($n > 1$) do not produce moving boundaries. When the dynamic yield stress exceeds the static yield stress and the fluid behaves like a rigid body in the static regime, the governing equations are nonlinear and parabolic: there is a moving interface separating the static and flowing layers. However, this interface does not start moving spontaneously when a body force is applied; part of the layer must be sufficiently destabilised.

In the literature on geophysical fluid mechanics, the Herschel-Bulkley equation has often been used to model snow avalanches and debris flows [2,3,34–39]. When the material flows over an erodible static layer made of the same material, the incoming flow is often expected to gradually erode the static layer [2–4]. The classic Herschel-Bulkley equation (in which the material behaves like a rigid body in the absence of shear rate) and its extended form (in which the material behaves like a viscoelastoplastic material) produce interfaces (between the static and flowing regions) that move at infinite speed [7,8] (see Section 3). This means that the entire static layer is mobilised instantaneously when its thickness H exceeds the critical depth $h_c = \tau_c/(\rho g \sin \theta)$. For this reason, simple Herschel-Bulkley fluids are not suited to basal entrainment problems. Adding some thixotropy, i.e. considering static and dynamic yield stresses, produces interfaces moving at a finite velocity (see Section 4). In our problem, the material must be sufficiently destabilised for the interface to propagate, and the condition (23) is rather a stringent one, as a large part of the layer must be disturbed initially. In conclusion, therefore, even if this formulation has some advantages over the classic Herschel-Bulkley equation, it is not without its problems. It is also noteworthy that many real-world scenarios involve elongated flows over shallows erodible layers. If erosion occurs quickly—as shown here by the estimates of the time required for setting in motion t_c —then a radical but efficient assumption is that the whole basal layer is set in motion when the surge passes over it. We explored this scenario in a companion paper and found that it led to a reasonably good prediction of surge dynamics for the dam-break problem [40].

Another topical issue in geophysical fluid dynamics hinges upon the proper way of dealing with basal entrainment in mass and momentum depth-averaged equations. This issue lacks a consensus [9]. In the present paper, we showed that when using depth-averaged equations and Herschel-Bulkley fluids, the problem is closed (i.e. we do not need further closure equations) in the absence of basal slip. However, the solution is physically inconsistent—the flowing layer does not grow, but shrinks. In the presence of basal slip, this inconsistency can be removed, but two closure equations must be provided (one for the entrainment rate and the other for basal slip). One merit of Stokes' third problem is that it sheds light on the nature of the moving interface between sheared and unsheared materials. Many investigations (reported by [9]) have considered this interface to behave like a shock wave, whose dynamics could be prescribed independently of what happens inside the flowing layer. In both the present paper and a

recent related contribution on Drucker–Prager fluids [4], the interface is a part of the problem to be solved, and thus there is only a small possibility that we can relate its dynamic features to its bulk quantities (such as flow depth and depth-averaged velocity).

Acknowledgements

The work presented here was supported by the Swiss National Science Foundation under Grant No. 200021_146271/1, a project called “Physics of Basal Entrainment.” The authors are grateful to two anonymous reviewers for their feedback and to Guillaume Ovarlez and Anne Mangeney for discussions. The scripts used for computing Figs. 2,3,6–8, B.11, and B.12 are available from the figshare data repository: dx.doi.org/10.6084/m9.figshare.3496754.v1.

Appendix A. Characteristic problem

In this appendix, we show how the problem (12)–(13) can be cast in characteristic form and how this can be used to solve the problem numerically.

The initial boundary value problem (12)–(13) addressed in Section 3 can be cast in matrix form

$$\frac{\partial}{\partial t} \mathbf{X} + \mathbf{A} \cdot \frac{\partial}{\partial z'} \mathbf{X} = \mathbf{B} \tag{A.1}$$

subject to $u = 0$ at $z' = 0$, $\tau = 0$ at $z' = 1$, and $\tau = u = 0$ at $t = 0$. The hat annotation has been removed for the sake of simplicity. We have introduced

$$\mathbf{X} = \begin{pmatrix} u \\ \tau \end{pmatrix}, \mathbf{A} = - \begin{pmatrix} 0 & \text{Re}^{-1} \\ \text{De}^{-1} & 0 \end{pmatrix}, \text{ and } \mathbf{B} = \begin{pmatrix} \text{Re}^{-1} \\ -\text{De}^{-1} F(\tau) \end{pmatrix}. \tag{A.2}$$

We now introduce the Riemann variables $r = -\eta u + \tau$ and $s = \eta u + \tau$, where $\eta = \sqrt{\text{Re}/\text{De}}$. The eigenvalues of \mathbf{A} are constant and of opposite sign: $\pm \lambda$ with $\lambda = 1/\sqrt{\text{ReDe}}$, which means that the characteristic curves are straight lines (see Fig. A.9): $z' = \pm \lambda t + c$ (with c a constant). The characteristic form of (A.1) is

$$\frac{dr}{dt} = R(\tau) = -\lambda - \text{De}^{-1} F(\tau) \text{ along } \frac{dz'}{dt} = \lambda, \tag{A.3}$$

$$\frac{ds}{dt} = S(\tau) = \lambda - \text{De}^{-1} F(\tau) \text{ along } \frac{dz'}{dt} = -\lambda, \tag{A.4}$$

with the boundary conditions $r = s$ at $z' = 0$ and $r = -s$ at $z' = 1$. The initial conditions are $r = s = 0$ at $t = 0$. As the source term is

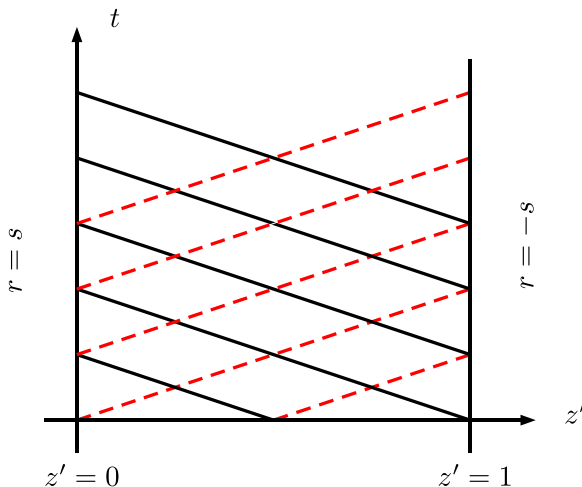


Fig. A.9. Characteristic diagram showing the two families of characteristic curves.

nonlinear in τ , this system of equations has no analytical solution, but it lends itself more readily to numerical solutions.

The domain is divided into $N - 1$ intervals whose nodes are $z_i = i\delta x$, with $\delta z = 1/N$, for $0 \leq i \leq N$. The center of each interval is $z_{i+1/2} = (z_i + z_{i+1})/2$. The numerical integration of the system (A.3)–(A.4) involves two steps. We assume that we know the values r_i^{2k} and s_i^{2k} of r and s at each node at time $t = 2k\delta t$ with $\delta t = \delta x/2/\lambda$. At time $t + \delta t$, a first-order discretisation of (A.3)–(A.4) is

$$r_{i+1/2}^{2k+1} = r_i^{2k} + R(\tau_i^{2k})\delta t \text{ and } s_{i+1/2}^{2k+1} = s_{i+1/2}^{2k} + S(\tau_{i+1}^{2k})\delta t, \tag{A.5}$$

for $0 \leq i \leq N - 1$. At time $t + 2\delta t$, we have

$$r_i^{2k+2} = r_{i-1/2}^{2k+1} + R(\tau_{i-1/2}^{2k+1})\delta t \text{ and } s_i^{2k+2} = s_{i+1/2}^{2k+1} + S(\tau_{i+1/2}^{2k+1})\delta t, \tag{A.6}$$

for $1 \leq i \leq N - 1$, while at the boundaries, we have

$$r_0^{2k+2} = s_0^{2k+2} \text{ and } s_0^{2k+2} = s_{1/2}^{2k+1} + S(\tau_{1/2}^{2k+1})\delta t, \tag{A.7}$$

and

$$r_N^{2k+2} = r_{N-1/2}^{2k+1} + R(\tau_{N-1/2}^{2k+1})\delta t \text{ and } s_N^{2k+2} = -r_N^{2k+2}. \tag{A.8}$$

At each time step, the velocity and shear stress are thus

$$\tau_i^j = \frac{1}{2}(r_i^j + s_i^j) \text{ and } u_i^j = \frac{1}{2\eta}(s_i^j - r_i^j). \tag{A.9}$$

Appendix B. Numerical solution to the Stefan-like problem

In this appendix, we propose a finite-difference algorithm for the Stefan-like problem (16). Various techniques have been developed to solve Stefan problems [33,41–44], but the change in the boundary condition (19) (the gradient is constant in our problem, whereas it is linearly related to interface velocity in the classical Stefan problem) makes the numerical problem more difficult. Here we take inspiration from Morland [45] (see Section B.1). By modifying the boundary condition (19) (and thus returning to the original Stefan problem), we can work out a similarity solution which is then used to test the algorithm accuracy (see Section B.2).

B.1. Numerical scheme

For the sake of brevity, we omit the hat annotation in this appendix. We make the following change of variable

$$u(z, t) = \tilde{u}(z, s),$$

where time has been replaced by s . Assuming that $s(t)$ is a continuous monotonic function of time and $\dot{s}(t) > 0$, the Jacobian of the transformation is non-zero. The advantage of this change of variable is that the front position appears explicitly in the governing equations and the domain of integration now has known boundaries. We must solve the following initial boundary value problem

$$\text{Re}\alpha(s) \frac{\partial \tilde{u}}{\partial s} = 1 + \frac{\partial^2 \tilde{u}}{\partial z^2} \text{ with } \alpha(s) = \frac{ds}{dt} \tag{B.1}$$

subject to the boundary conditions at the free surface

$$\frac{\partial \tilde{u}}{\partial z}(0, s) = 0. \tag{B.2}$$

There is a moving boundary at $z = s(t)$ for which the no-slip condition holds

$$\tilde{u}(s, s) = 0. \tag{B.3}$$

The stress continuity (5) across this interface gives

$$\frac{\partial \tilde{u}}{\partial z}(s, s) = -\dot{\gamma}_c \text{ with } \dot{\gamma}_c = \tau_0 - \text{Bi} > 0. \tag{B.4}$$

The initial condition is

$$\tilde{u}(z, s_0) = \tilde{u}_0(z) \text{ for } 0 \leq z \leq s_0. \tag{B.5}$$

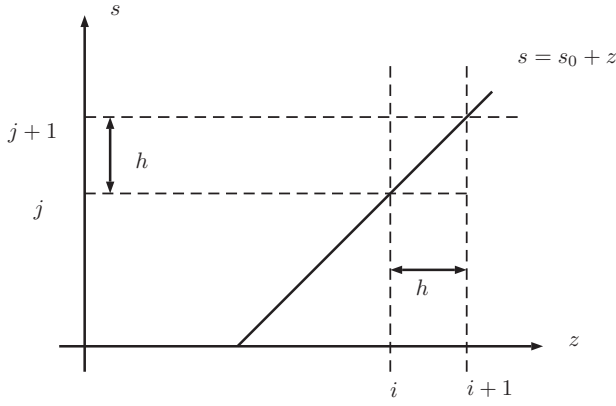


Fig. B.10. Domain of integration. The change of variable $t \rightarrow s$ makes it possible to work on a fixed domain, where the upper bound s is fixed in advance: $s = s_0 + z$.

Once the solution $\tilde{u}(x, s)$ has been calculated, we can return to the original variables by integrating $\alpha(s)$

$$t = \int_{s_0}^s \frac{ds'}{\alpha(s')} \quad (\text{B.6})$$

The numerical strategy is the following. The domain of integration is discretised using a uniform rectangular grid with a fixed mesh size h . Time t , and thus parameter α , are calculated at each iteration so that the front has moved a distance h (see Fig. B.10). The value of the numerical solution at $z = ih$ and $s = jh$ is denoted by u_i^j . The front position at time step jh is denoted by $s^j = s_0 + jh$. We use an implicit finite-difference scheme for discretising the spatial derivatives and an explicit forward Euler for the time derivative in Eq. (B.1):

$$-ru_{i-1}^{j+1} + (2r + a^{j+1})u_i^{j+1} - ru_{i+1}^{j+1} = h^2 + (1-r)u_{i-1}^j + (a^j - 2(1-r))u_i^j + (1-r)u_{i+1}^j, \quad (\text{B.7})$$

for $0 \leq i \leq j+1$. We have introduced the weighting coefficient $0 < r \leq 1$ and $a^j = \text{Re } h\alpha^{j+1/2}$, where $\alpha^{j+1/2} = k\alpha^j + (1-k)\alpha^{j+1}$. In practice, we take $r = 1/2$ (Crank-Nicolson scheme) and $0 \leq k \leq 0.25$.

The scheme (B.7) involves ghost cells at $i = -1$ (for time j and $j+1$) and $i = j+1$ (for time j). For the free surface, we introduce the ghost cell u_{-1}^j . The gradient is approximated as $\partial_z u = (u_1^j - u_{-1}^j)/(2h) + o(h^2)$. The boundary condition (B.2) implies $u_{-1}^j = u_1^j$. Taking Eq. (B.7) for $i = 0$, we then get

$$(a^{j+1} + 2r)u_0^{j+1} - 2ru_1^{j+1} = h^2 + 2(1-r)u_1^j + (a^{j+1} - 2(1-r))u_0^j.$$

For the interface, we introduce another ghost cell u_{j+2}^{j+1} (at time $j+1$). The boundary condition (B.4) implies $u_{j+2}^{j+1} = u_j^{j+1} - 2h\dot{\gamma}_c$. Taking Eq. (B.7) for $i = j+1$ leads to

$$(a^{j+1} + 2r)u_{j+1}^{j+1} - 2ru_j^{j+1} = h^2 - 2h\dot{\gamma}_c + 2(1-r)u_j^j + (a^{j+1} - 2(1-r))u_{j+1}^j.$$

The scheme involves the value u_{j+1}^j outside the domain of integration. We use a second-order Taylor-series extrapolation

$$u(s+h, s) = u(s, s) + hu_z(s, s) + \frac{h^2}{2}u_{zz}(s, s) + o(h^2).$$

We use the boundary condition (B.3) ($u(s, s) = 0$), the boundary condition (B.4) ($u_z(s, s) = -\dot{\gamma}_c$), and the governing equation (B.1) together with (21) ($u_{zz}(s, s) = \text{Re } \alpha\dot{\gamma}_c - 1$). We then obtain

$$u_{j+1}^j = -\dot{\gamma}_c h - \frac{1}{2}h^2(1 - \text{Re } \alpha^j \dot{\gamma}_c). \quad (\text{B.8})$$

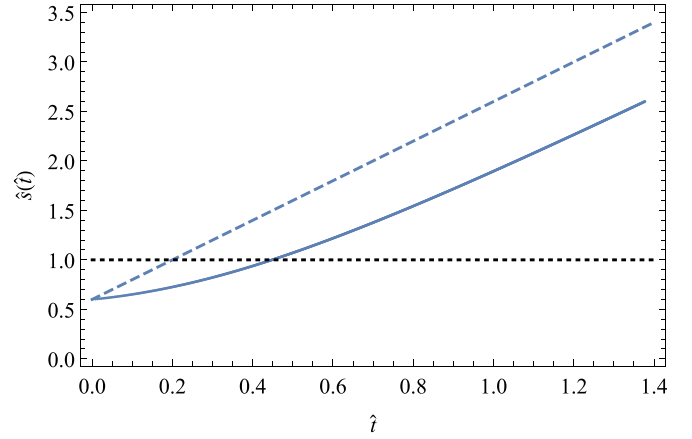


Fig. B.11. Interface position $\hat{s}(\hat{t})$ over time. The solid line shows the numerical solution to system (16)–(19) whereas the dashed line represents the approximate solution (27). Numerical solution for $\text{Bi} = 0.5$, $\hat{\tau}_0 = 1$, $\hat{\gamma}_c = \hat{\tau}_0 - \text{Bi} = 0.5$ and $\text{Re} = 1$. We used the parameters $r = 0.5$ and $k = 0$.

Note that under some conditions, the interface velocity exhibits oscillations. This may be cured by discretising the boundary conditions as follows. The boundary condition (B.2) is discretised by

$$ru_2^{j+1} - ru_1^{j+1} = (1-r)u_1^j + (1-r)u_2^j, \quad (\text{B.9})$$

while the boundary condition (B.4) gives

$$ru_{j+1}^{j+1} - ru_{j-1}^{j+1} = (1-r)u_{j-1}^j + (1-r)u_{j+1}^j - 2h\dot{\gamma}_c. \quad (\text{B.10})$$

At time step $j+1$, we thus have to solve the system of $j+2$ equations

$$\mathbf{P}(r, h, \alpha^{j+1}) \cdot \mathbf{U}^{j+1} = \mathbf{Q}(r, h, \alpha^{j+1}) \cdot \mathbf{U}^{j+1} + \mathbf{R}(h, \dot{\gamma}_c),$$

where \mathbf{P} and \mathbf{Q} are tridiagonal matrices and \mathbf{R} is a constant vector, whose entries are given by Eqs. (B.9)–(B.8). The coefficient α^{j+1} is adjusted until the boundary condition (B.3) is satisfied: $u_{j+1}^{j+1} = 0$. To that end, we use the secant method:

$$s^{j+1, (k+1)} = s^{j+1, (k)} - \frac{s^{j+1, (k)} - s^{j+1, (k-1)}}{u_{j+1}^{j+1, (k)}(s^{j+1, (k)}) - u_{j+1}^{j+1, (k-1)}(s^{j+1, (k-1)})}$$

where $s^{j+1, (k+1)}$ the k th iteration to find s^{j+1} . The stopping criterion is

$$|s^{j+1, (k+1)} - s^{j+1, (k)}| < h^2 |s^{j+1, (k)}|.$$

Usually, only a few iterations are required to find α^{j+1} . To estimate time t , we integrate Eq. (B.6) numerically by approximating the integrand using a second-order polynomial. We can then iteratively calculate t^j

$$t^{j+1} = t^{j-1} + \frac{h}{3} \left(\frac{1}{\alpha^{j+1}} + \frac{4}{\alpha^j} + \frac{1}{\alpha^{j-1}} \right).$$

B.2. Testing the algorithm

The initial boundary value problem (B.1)–(B.4) has no similarity solution, but if we replace the boundary (B.4) with

$$\frac{\partial \tilde{u}}{\partial z}(s, s) = -as, \quad (\text{B.11})$$

where $0 < a < 1$ is a free parameter, then we can work out a similarity solution

$$u(x, t) = tU(\eta) \text{ with } \eta = \frac{x}{b\sqrt{t}}, b = \sqrt{2 \frac{1-a}{a}}, \quad (\text{B.12})$$

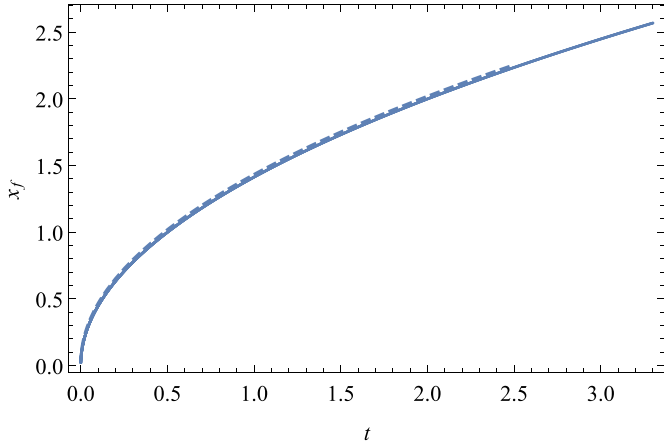


Fig. B.12. Comparison of the numerical solution (solid line) and the analytical solution (dashed line) given by Eq. (B.13). Simulation for $a = 0.5$ and $h = 10^{-3}$.

and

$$U(\eta) = \frac{b^2}{2 + b^2} (1 - \eta^2).$$

The front position is given by

$$s(t) = s_0 + b\sqrt{t}. \quad (\text{B.13})$$

The algorithm of Section B.1 was adapted to take the change in the boundary condition into account. Fig. B.12 shows a comparison between the numerical solution and the analytical solution (B.13). The initial condition is the solution (B.11) reached by u at time $t_0 = (s_0/b)^2$. The initial front position is arbitrarily set to $s_0 = 50h$. There is a fairly good agreement, but even if the algorithm is a second order one, errors accumulate. In the example in Fig. B.12, the error reaches 0.8% after 10,000 iterations.

Appendix C. Depth-averaged equations

In this appendix, we derive the depth-averaged equations for a Bingham fluid and erodible bottoms. As the derivation of these equations is classic, we will look especially at the changes induced by the erodible bottom. The reader is referred to [35,46–48] for a more complete derivation of the depth-averaged equations for Bingham fluids, and to [9] for the treatment of mass exchanges.

A Bingham fluid flows over an erodible bottom, as sketched in Fig. C.13. The free surface is located at $z = s(x, t)$; the basal layer lies at $z = b(x, t)$. The free surface is a material boundary. The basal layer is a non-material interface whose displacement speed in the normal direction \mathbf{n}_b is denoted by $v_f \mathbf{n}_b$, where \mathbf{n}_b is the unit normal.

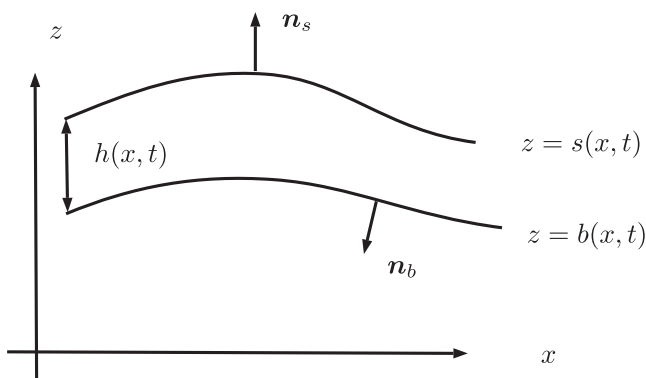


Fig. C.13. Flowing layer bounded by two interfaces, $z = s(x, t)$ and $z = b(x, t)$.

For the dynamic boundary conditions, we assume that there is no stress acting on the free surface: $\boldsymbol{\sigma} \cdot \mathbf{n}_s = 0$ where \mathbf{n}_s is the unit normal pointing outward. For the basal layer, the Rankine-Hugoniot relation (3) holds, and in the absence of slip, this relation implies the stress continuity across the interface (5).

For the kinematic conditions, we introduced the functionals, F_b and F_s , that are implicit representations of the base and free-surface interfaces, respectively [12]: $F_b = -z + b(x, t) = 0$ and $F_s = z - s(x, t) = 0$. The functionals are defined such that the unit normal $\mathbf{n}_i = \nabla F_i / |\nabla F_i|$ (with $i = b, s$) points outward from the flowing layer. For the free surface, the kinematic condition is

$$F_s = 0 \text{ and } \frac{\partial F_s}{\partial t} + \mathbf{u}_s \cdot \nabla F_s = 0, \quad (\text{C.1})$$

where $\mathbf{u}_s = (u_s, w_s)$ is the fluid velocity at the free surface. For the basal surface, the kinematic condition involves the interface velocity $\mathbf{v}_b = \mathbf{u}_b + v_f \mathbf{n}_b$, where $\mathbf{u}_b = (u_b, w_b)$ is the fluid velocity at the base.

$$F_b = 0 \text{ and } \frac{\partial F_b}{\partial t} + \mathbf{v}_b \cdot \nabla F_b = 0 \Rightarrow \frac{\partial F_b}{\partial t} + u_b \frac{\partial F_b}{\partial x} = w_b - v_f |\nabla F_b| \quad (\text{C.2})$$

Integrating the local mass balance equation over depth $h = s - b$ gives

$$\int_b^s \left(\frac{\partial u}{\partial x} + \frac{\partial w}{\partial z} \right) dz = \frac{\partial}{\partial x} (h\bar{u}) - \left[u \frac{\partial z}{\partial x} - w \right]_b^s = 0, \quad (\text{C.3})$$

where we have introduced the depth-averaged velocity

$$\bar{u}(x, t) = \frac{1}{h} \int_b^s u(x, z, t) dz.$$

Making use of Eqs. (C.1) and (C.2), we obtain

$$\frac{\partial}{\partial t} h + \frac{\partial}{\partial x} (h\bar{u}) = e, \quad (\text{C.4})$$

with $e = v_f |\nabla F_b|$ the entrainment rate. We now consider the momentum balance equation in the x -direction

$$\frac{\partial u}{\partial t} + u \frac{\partial u}{\partial x} + w \frac{\partial u}{\partial z} = g \sin \theta + \frac{1}{\rho} \left(\frac{\partial \sigma_x}{\partial x} + \frac{\partial \tau}{\partial z} \right), \quad (\text{C.5})$$

whose integration over the flow depth provides

$$\begin{aligned} \frac{\partial}{\partial t} (h\bar{u}) + \frac{\partial}{\partial x} (h\bar{u}^2) + \left[u \left(\frac{\partial z}{\partial t} + u \frac{\partial z}{\partial x} - w \right) \right]_b^s \\ = gh \sin \theta - \frac{\tau_b}{\rho} + \frac{1}{\rho} \int_b^s \frac{\partial \sigma_x}{\partial x} dz, \end{aligned} \quad (\text{C.6})$$

where τ_b is the basal shear stress. Making use of Eqs. (C.1) and (C.2), we obtain

$$\frac{\partial}{\partial t} (h\bar{u}) + \frac{\partial}{\partial x} (h\bar{u}^2) = u_b e + gh \sin \theta - \frac{\tau_b}{\rho} + \frac{1}{\rho} \int_b^s \frac{\partial \sigma_x}{\partial x} dz. \quad (\text{C.7})$$

The depth-averaged equations are not closed. The relationship between \bar{u} and \bar{u}^2 , the bottom shear-stress τ_b , the depth-averaged normal, and the entrainment rate e stress must be specified. In the present context, we will focus on the determination of τ_b . One common approach is to assume that in gradually varied flows, the bottom shear-stress is the same as that exerted by a steady uniform flow with the same flow depth and depth-averaged velocity [1,35,47], which leads to the following expression

$$\tau_b = \tau_c + 2\kappa \frac{\bar{u}}{f(h)} \text{ with } h = (h - h_c) \left(\frac{2}{3} + \frac{h_c}{3h} \right), \quad (\text{C.8})$$

with $h_c = \tau_c / (\rho g \sin \theta)$ the critical depth. The problem with this equation is that it holds for slightly non-uniform flows and flow

depths in excess of h_c . Alternative approaches have been developed, however they end up with different expressions for τ_b . For instance, Pastor et al. [49] proposed a second-order polynomial approximation to the bottom shear-stress. Fernández-Nieto et al. [48] presented a more rigorous treatment of the depth-averaged equations based on asymptotic expansions of the velocity field. They proposed an expression for τ_b that supplements (C.8) with higher-order spatial derivatives of h .

References

- [1] C. Ancey, Plasticity and geophysical flows: a review, *J. Non-Newtonian Fluid Mech.* 142 (2007) 4–35.
- [2] M.E. Eglit, A.E. Yakubenko, Numerical modeling of slope flows entraining bottom material, *Cold Reg. Sci. Technol.* 108 (2014) 139–148.
- [3] D. Issler, Dynamically consistent entrainment laws for depth-averaged avalanche models, *J. Fluid Mech.* 759 (2014) 701–738.
- [4] B. Bouchut, I.R. Ionescu, A. Mangeney, An analytic approach for the evolution of the static/flowing interface in viscoplastic granular flows, *Comm. Math. Sci.* 14 (2016) 2101–2126.
- [5] E.J. Watson, Boundary-layer growth, *Proc. R. Soc. London ser. A* 231 (1955) 104–116.
- [6] P.G. Drazin, N. Riley, *The Navier–Stokes Equations: A Classification of Flows and Exact Solutions*, Cambridge University Press, Cambridge, 2006.
- [7] H. Pascal, Propagation of disturbances in a non-newtonian fluid, *Physica D* 39 (1989) 262–266.
- [8] B.R. Duffy, D. Pritchard, S.K. Wilson, The shear-driven rayleigh problem for generalised newtonian fluids, *J. Non-Newtonian Fluid Mech.* 206 (2014) 11–17.
- [9] R.M. Iverson, C. Ouyang, Entrainment of bed material by earth-surface mass flows: review and reformulation of depth-integrated theory, *Rev. Geophys.* 53 (2015) 27–58.
- [10] N.J. Balmforth, Y. Forterre, O. Pouliquen, The viscoplastic stokes layer, *J. Non-Newtonian Fluid Mech.* 158 (2009) 46–53.
- [11] P. Chadwick, *Continuum Mechanics: Precise Theory and Problems*, Dover, Mineola, 1999.
- [12] K. Hutter, K. Jöhnk, *Continuum Methods of Physical Modeling*, Springer, Berlin, 2004.
- [13] L. Fraccarollo, H. Capart, Riemann wave description of erosional dam break flows, *J. Fluid Mech.* 461 (2002) 183–228.
- [14] R.M. Iverson, Elementary theory of bed-sediment entrainment by debris flows and avalanches, *J. Geophys. Res.* 117 (2012) F03006.
- [15] G. Ovarlez, S. Rodts, X. Chateau, P. Coussot, Phenomenology and physical origin of shear localization and shear banding in complex fluids, *Rheol. Acta* 48 (2009) 831–844.
- [16] T. Divoux, M.A. Fardin, S. Manneville, S. Lerouge, Shear banding of complex fluids, *Annu. Rev. Fluid Mech.* 48 (2016) 81–103.
- [17] P. Coussot, Yield stress fluid flows: a review of experimental data, *J. Non-Newtonian Fluid Mech.* 211 (2014) 31–49.
- [18] N.J. Balmforth, I.A. Frigaard, G. Ovarlez, Yielding to stress: recent developments in viscoplastic fluid mechanics, *Annu. Rev. Fluid Mech.* 46 (2014) 121–146.
- [19] G. Ovarlez, Q. Barral, P. Coussot, Three-dimensional jamming and flows of soft glassy materials, *Nature Mater.* 9 (2010) 115–119.
- [20] P. Coussot, Q.D. Nguyen, H.T. Huynh, D. Bonn, Viscosity bifurcation in thixotropic, yielding fluids, *J. Rheol.* 46 (2002) 573–590.
- [21] F.d. Cruz, F. Chevoir, D. Bonn, P. Coussot, Viscosity bifurcation in granular materials, foams, and emulsions, *Phys. Rev. E* 66 (2002) 051305.
- [22] P. Møller, A. Fall, V. Chikkadi, D. Derks, D. Bonn, An attempt to categorize yield stress fluid behaviour, *Phil. Trans. Roy. Soc. London A* 367 (2009) 5139–5155.
- [23] G. Picard, A. Ajdari, L. Bocquet, F. Lequeux, Simple model for heterogeneous flows of yield stress fluids, *Phys. Rev. E* 66 (2002) 051501.
- [24] J. Mewis, N.J. Wagner, Thixotropy, *Adv. Colloid Interface Sci.* 147–148 (2009) 214–227.
- [25] G. Ovarlez, S. Rodts, A. Ragouilliaux, P. Coussot, J. Goyon, A. Colin, Wide-gap couette flows of dense emulsions: local concentration measurements, and comparison between macroscopic and local constitutive law measurements through magnetic resonance imaging, *Phys. Rev. E* 78 (2008) 036307.
- [26] G. Ovarlez, K. Krishan, S. Cohen-Addad, Investigation of shear banding in three-dimensional foams, *EPL* 91 (2010) 68005.
- [27] G. Ovarlez, S. Cohen-Addad, K. Krishan, J. Goyon, P. Coussot, On the existence of a simple yield stress fluid behavior, *J. Non-Newtonian Fluid Mech.* 193 (2013) 68–79.
- [28] O. Thual, L. Lacaze, Fluid boundary of a viscoplastic Bingham flow for finite solid deformations, *J. Non-Newtonian Fluid Mech.* 165 (2010) 84–87.
- [29] P. Saramito, A new elastoviscoplastic model based on the Herschel–Bulkley viscoplastic model, *J. Non-Newtonian Fluid Mech.* 158 (2009) 154–161.
- [30] J.G. Oldroyd, On the formulation of rheological equations of state, *Proc. R. Soc. London ser. A* 200 (1950) 523–541.
- [31] I. Cheddadi, P. Saramito, F. Graner, Steady Couette flows of elastoviscoplastic fluids are nonunique, *J. Rheol.* 56 (2012) 213–239.
- [32] L. Lacaze, A. Filella, O. Thual, Steady and unsteady shear flows of a viscoplastic fluid in a cylindrical couette cell, *J. Non-Newtonian Fluid Mech.* 220 (2015) 126–136.
- [33] G. Marshall, A front tracking method for one-dimensional moving boundary problems, *SIAM J. Sci. Stat. Comput.* 7 (1986) 252–263.
- [34] C. Ancey, Modélisation des avalanches denses, approches théorique et numérique, *La Houille Blanche* 5–6 (1994) 25–39.
- [35] P. Coussot, *Mudflow Rheology and Dynamics*, Balkema, Rotterdam, 1997.
- [36] M.A. Kern, F. Tiefenbacher, J.N. McElwaine, The rheology of snow in large chute flows, *Cold Reg. Sci. Technol.* 39 (2004) 181–192.
- [37] E. Bovet, B. Chiaia, L. Preziosi, A new model for snow avalanche dynamics based on non-newtonian fluids, *Meccanica* 45 (2010) 753–765.
- [38] J. Rougier, M.A. Kern, Predicting snow velocity in large chute flows under different environmental conditions, *J. R. Stat. Soc. Ser. C Appl. Stat.* 59 (2010) 737–760.
- [39] C. Ancey, Gravity Flow on Steep Slope, in: E. Chassignet, C. Cenedese, J. Verron (Eds.), *Buoyancy Driven Flows*, Cambridge University Press, New York, 2012, pp. 372–432.
- [40] B.M. Bates, C. Ancey, The dambreak problem for eroding viscoplastic fluids, *J. Non-Newtonian Fluid Mech.* accepted for publication (0000).
- [41] J. Crank, *The Mathematics of Diffusion*, Oxford University Press, Oxford, 1975.
- [42] R.S. Gupta, D. Kumar, Variable time step methods for one-dimensional Stefan problem with mixed boundary condition, *Int. J. Heat Mass Trans.* 24 (1981) 251–259.
- [43] N.S. Asaithambi, A variable time step Galerkin method for a one-dimensional Stefan problem, *Appl. Math. Comput.* 81 (1997) 189–200.
- [44] S.L. Mitchell, M. Vynnycky, Finite-difference methods with increased accuracy and correct initialization for one-dimensional Stefan problems, *Appl. Math. Comput.* 215 (2009) 1609–1621.
- [45] L.W. Morland, A fixed domain method for diffusion with a moving boundary, *J. Eng. Math.* 16 (1982) 259–269.
- [46] J.M. Piau, Flow of a yield stress fluid in a long domain. Application to flow on an inclined plane, *J. Rheol.* 40 (1996) 711–723.
- [47] X. Huang, M.H. García, A perturbation solution for Bingham-plastic mudflows, *J. Hydraul. Eng.* 123 (1997) 986–994.
- [48] E.D. Fernández-Nieto, P. Noble, J.P. Vila, Shallow water equation for non-Newtonian fluids, *J. Non-Newtonian Fluid Mech.* 165 (2010) 712–732.
- [49] M. Pastor, M. Quecedo, E. González, M.I. Herreros, J.A. Fernández, P. Mira, Simple approximation to bottom friction for Bingham fluid depth integrated models, *J. Hydraul. Eng.* 130 (2004) 149–155.